**Dalton
Transactions**

Protonation of bridging sulfur in cubanoid Fe4S4 clusters causes large geometric changes: the theory of geometric and electronic structure.

DT-ART-12-2014-003681 R2

Protonation of bridging sulfur in cubanoid Fe_4S_4 clusters causes large geometric changes: the theory of geometric and electronic structure.

Ian Dance

School of Chemistry, University of New South Wales, Sydney 2052, Australia.

i.dance@unsw.edu.au

Abstract

Density functional calculations indicate that protonation of a μ_3-S atom in cubanoid clusters $[Fe_4S_4X_4]^{2-}$ leads to a large extension of one Fe-S(H) bond such that the SH ligand is doubly-bridging, μ-SH. Triply-bridging SH in these clusters is unstable, relative to μ-SH. The theory for the geometric and electronic structures of the protonated $[Fe_4S_4X_4]^{2-}$ clusters (X = Cl, SEt, SMe, SPh, OMe, OPh) is presented in this paper. The principal results are (1) the unique Fe atom in $[Fe_4S_3(SH)X_4]^-$ is three-coordinate, with planar or approximately planar stereochemistry, (2) approximately equi-energetic *endo* and *exo* isomers occur for μ-SH, (3) the structural changes caused by protonation reverse without barrier on deprotonation, (4) the most stable electronic states have S=0 and oppositely signed spin densities on the Fe atoms bearing the μ-SH bridge, (5) interconversions between *endo* and *exo* isomers, and between ground and excited states, occur through concerted lengthenings and shortenings of Fe-S(H) interactions, on relatively flat energy surfaces, (6) protonation of an X ligand does not change the characteristics of protonation of μ_3-S. Experimental tests of this theory are suggested, and applications discussed.

Introduction

The cubanoid Fe_4S_4 cluster core, with triply-bridging sulfide ligands, is a fundamental entity in bio-inorganic chemistry.[1-6] This paper describes theoretical results on the consequences of protonation of a μ_3-S atom in these clusters $[Fe_4S_4X_4]^{2-}$. The question of protonation $[Fe_4S_4X_4]^{2-}$ has two main origins. The first, chronologically, is the acid-catalysed substitution of $[Fe_4S_4X_4]^{2-}$, eq (1), and the question of the mechanism of this catalysis. Secondly, the protonation of a related cluster, the FeMo-co active site of nitrogenase, is part of proposed mechanisms of its enzymatic functions.

The active site of the enzyme nitrogenase[7-13] is the iron-molybdenum cofactor (FeMo-co), the core of which is a metal sulfide cluster with composition Fe_7MoS_9C.[14,15] This cluster contains the topological elements of two vertex-fused cubanoid clusters, and it contains six μ_3-S groups (Fig 1a). Theoretical investigations of the mechanism of nitrogenase led to the postulate that one of these μ_3-S groups, S3B, is protonated as part of the proton supply required for the hydrogenation reactions effected by nitrogenase.[16-18] These calculations showed that when this S atom bonded to three metal atoms is protonated, one of the S-M bonds elongates greatly (by > 0.7Å) to the extent of severance. The stable form of protonated S is doubly bridging μ-SH, not μ_3-SH. Four stable isomers of protonated S3B in FeMo-co are depicted in Fig 1b.
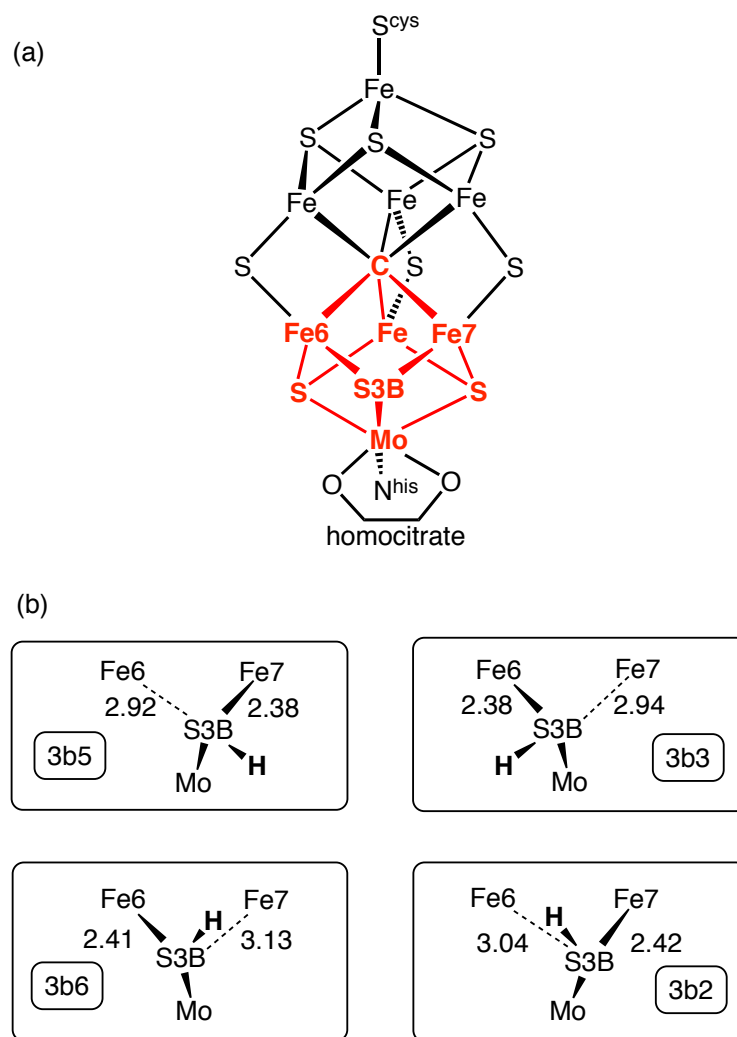
Fig 1. (a) The structure of the Fe_7MoS_9C cluster that is the core the FeMo-co active site of nitrogenase. The linked cubanoid topology is emphasised through red/black colouration. (b) Four stable conformers for protonated S3B, with distances (Å) to Fe6, Fe7: S3B-H is doubly-bridging.[17]

Experimental knowledge of the protonation of μ_3-S in $[Fe_4S_4X_4]^{2-}$ clusters derives mainly from the work of Henderson *et al*, who recognised that protonation of $[Fe_4S_4X_4]^{2-}$ clusters accelerated the rates of reactions in which X is substituted by another ligand Y (eq 1), and undertook extensive kinetic investigations of the mechanism of this catalysis.[19,20] Protonation of μ_3-S in $[Fe_4S_4X_4]^{2-}$ is a central hypothesis of the mechanistic interpretations of the kinetic data. The results for nitrogenase prompted theoretical investigations of the protonation of $[Fe_4S_4X_4]^{2-}$, and the finding was analogous: protonation of μ_3-S in $[Fe_4S_4X_4]^{2-}$ causes one S-Fe bond to elongate, such that the resulting protonated entity is μ-SH. Further, the severance of the S-Fe bond leaves that Fe under-coordinated, susceptible to nucleophilic attack by the incoming ligand Y, and by solvent MeCN. This new finding allowed a reinterpretation of the kinetic data for the reactions (1), and led to presentation of a modified mechanism consistent with all kinetic data, and theoretical simulations of the steps involved.[21,22]

$$[Fe_4S_4X_4]^{2-} + Y^- \xrightarrow[\text{catalysis}]{BH^+} [Fe_4S_4X_3Y]^{2-} + X^-$$

(1)
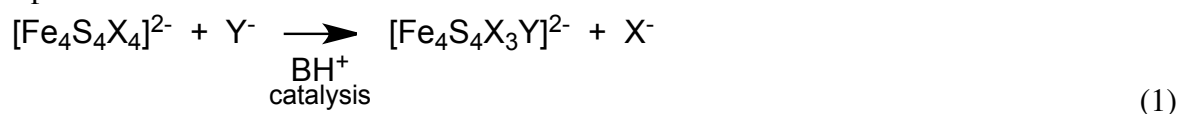
In this context it is significant that a search of the Cambridge Structural Database[23] showed six crystal structures for four chemical systems classified as containing $(\mu_3\text{-SH})M_3$, but in none of these is this structure characterised unambiguously.[24-26] In contrast, there are many instances of $(\mu$-

SH)M_2 with pyramidal stereochemistry. Kuwata and Hidai reached the same conclusion about the scarcity or non-existence of $(\mu_3\text{-SH})M_3$ in their review of M-SH complexes.[27]

This paper provides full details of density functional calculations of the protonated forms of $[Fe_4S_4X_4]^{2-}$ for X = Cl, OMe, OPh, SMe, SEt and SPh, including details of geometrical and electronic structure not previously reported.

Methodology

Density functional calculations use the methodology developed by Delley, implemented in the program DMol.[28-30] The accurate double numerical basis sets (dnp)[30] are used. The calculations are all electron, spin-unrestricted, with no imposed symmetry. The electronic structure of these clusters is conceived in terms of delocalised polar covalent bonding:[31] the Mulliken charges calculated here are +0.5 to + 0.6 on Fe, -0.5 to -0.6 on bridging S (similar calculated charges have been reported[32]). Electronic states are characterised by the signs and magnitudes (ca 3.1) of the spin densities of the Fe atoms (the calculated magnitudes of spin densities on other atoms are much smaller: <0.1 on sulfide atoms and ca 0.25 on the ligands). Unlike the electronic structure framework developed by Noodleman,[33,32] this model does not assume oxidation states or spin states for individual Fe atoms or for coupled Fe atom pairs, does not construct preliminary high spin states, and does not explicitly include Heisenberg spin coupling. The straightforward model used in DMol can accommodate the electronic structures associated with the various large and small disruptions to the Fe_4S_4 core geometry that occur in the reactions to be described. The DMol procedure allows for spin localisation to occur during bond breaking.[28]

The electronic states are controlled through input specifications of the signs and magnitudes of the Fe spin densities to be used at the start of the SCF convergence calculation: these spin densities are refined in the subsequent optimisation. The net spin S is controlled through occupations of the unrestricted α and β orbitals in the usual way. The blyp and pbe functionals were used, and results for both are presented. The main difference is that pbe calculates shorter distances. The real-space cutoff for calculation of atomic basis sets was 4.76Å; a fine integration mesh was used, with scf convergence to 10^{-6}; thermodynamic corrections were not applied, and the energies reported are potential energies. Transition states were obtained using the pragmatic method for exploration of minima and saddle points on the energy surface.[34,35]

As described in Supplementary Table S1, the atomic spin densities and atomic charges as calculated by the DMol methods used here and the broken symmetry procedure[32] have no significant differences. Additional validation information is provided in the Supplementary material.

Results

Background: electronic-geometric structure of $[Fe_4S_4X_4]^{2-}$

The bonding in $[Fe_4S_4X_4]^{2-}$ clusters is polar covalent and the electronic structure is delocalised.[31] The Fe_4S_4 cores are not exactly tetrahedral, but have a small D_{2d} distortion. In the ground electronic states with a net S=0 spin, the calculated spin densities on the Fe atoms are ca +3.1e or -3.1e, and there are necessarily four Fe--Fe pairs with oppositely-signed spin densities and two with same-signed spin densities. Accordingly, the Fe atom pairs with same-signed spins have a very small antibonding interaction, and are slightly longer than the other four. There are four shorter and eight longer Fe-S distances, in a compressed D_{2d} core structure.[36-39] Table 1 compares the D_{2d} dimensions of the core in its ground S=0 state, as observed and as calculated using the functionals blyp and pbe. The differentiation of the Fe--Fe distance pairs according to spin parity, and the D_{2d} distortion of the core, are calculated to be slightly more pronounced than observed. Both functionals provide acceptable replication of the observed distances. Excited S=1 states of $[Fe_4S_4X_4]^{2-}$ (including ferredoxin proteins where X = cysteine) are observed to be thermally

populated at ambient temperatures:[40,41,31] my calculations of S=1 states for $[Fe_4S_4Cl_4]^{2-}$, $[Fe_4S_4(SEt)_4]^{2-}$ and $[Fe_4S_4(SPh)_4]^{2-}$ place them 3 to 10 kcal mol^{-1} above the S=0 state, with distinct loss of D_{2d} symmetry in the magnitudes of the Fe spin densities and in the Fe-S, Fe--Fe dimensions.

Table 1. Observed and calculated core distances in the ground S=0 states of clusters $[Fe_4S_4X_4]^{2-}$. Numbers in parentheses are the number of distances averaged for core symmetry D_{2d}.

distance	$[Fe_4S_4Cl_4]^{2-}$	$[Fe_4S_4(SEt)_4]^{2-}$	$[Fe_4S_4(SPh)_4]^{2-}$
Fe--Fe (obs)	2.755 (2), 2.766 (4) [a]	2.776 (2), 2.732 (4) [b]	2.730(2), 2.739(4) [c]
Fe--Fe (blyp) [e]	2.92 (2), 2.81 (4)	2.85 (2), 2.80 (4)	2.86 (2), 2.75 (4)
Fe--Fe (pbe) [f]	2.81 (2), 2.72 (4)	2.74 (2), 2.71 (4)	2.77 (2), 2.67 (4)
Fe-S (obs)	2.260 (4), 2.295 (8) [a]	2.239 (4), 2.310 (8) [b]	2.267(4), 2.296(8) [c]
Fe-S (blyp) [e]	2.26 (4), 2.36 (8)	2.26 (4), 2.36 (8)	2.24 (4), 2.35 (8)
Fe-S (pbe) [f]	2.23 (4), 2.32 (8)	2.23 (4), 2.32 (8)	2.21 (4), 2.31 (8)

[a] ref [38]

[b] observed for $[Fe_4S_4(SCH_2Ph)_4]^{2-}$, ref [36].

[c] ref [37]

[e] calculated using functional blyp

[f] calculated using functional pbe

Structures of $[Fe_4S_3(SH)X_4]^-$

In silico addition of a proton to μ_3-S of $[Fe_4S_4X_4]^{2-}$ and energy optimisation leads to one or other of the $[Fe_4S_3(SH)X_4]^-$ structures shown in Scheme 1. Independent of the initial positioning of the proton near μ_3-S, there is elongation of one S-Fe bond, and formation of a pyramidal doubly-bridging SH group. One Fe atom (Fe^a, also denoted as the unique Fe atom) becomes three-coordinate, with approximately planar stereochemistry. Two configurational isomers exist for the pyramidal μ-SH group, and these isomers of $[Fe_4S_3(SH)X_4]^-$ are designated *endo* and *exo* relative to the elongated S--Fe^a vector (Scheme 1).
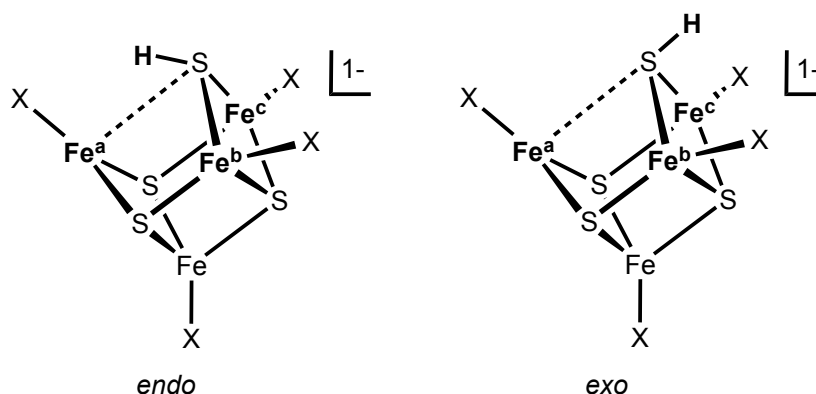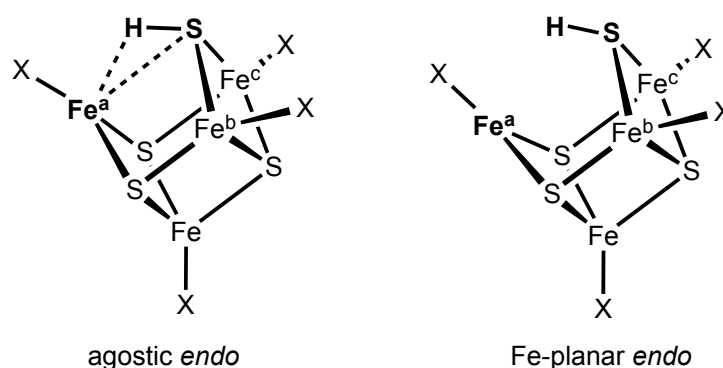

Scheme 1.

I have investigated the geometric and electronic properties of the *endo* and *exo* isomers of $[Fe_4S_3(SH)X_4]^-$ for X = Cl, OMe, OPh, SEt, SPh. The intrinsic properties of the protonated forms are most readily appreciated when X = Cl, because any effects arising from the conformations of substituents on X are absent, and there is no possibility of alternative or additional protonation of X.

Therefore results for X=Cl are presented and discussed first. Table 2 contains relative energies and key distances for the geometrical and electronic isomers of $[Fe_4S_3(SH)Cl_4]^-$. The variables are (a) the *endo* or *exo* conformations of μ-SH, (b) opposite- or same-signed signs for the Fe atoms supporting the μ-SH bridge, and (c) net spin S = 0 or 1. Values using density functionals blyp and pbe are provided (pbe values are enclosed [ ] throughout this paper).

The most stable structures have opposite spins across the bridge, net S=0, and similar energies for the *endo* and *exo* conformations. Next in the energy sequence are the *endo* and *exo* isomers with the same-signed spins across the bridge and S=0, and the S=1 states with opposite bridge spins. The least stable forms are those with the same bridge spins and S=1. Using abbreviated notation for the electronic states, this qualitative energy order is {opp / S=0} < {same / S=0} ≈ {opp / S=1} < {same / S=1}. Overall the *endo* isomers are slightly more stable than *exo*.

Looking first at the geometry of the ground state {opp / S=0} structures, the Fe^a--(SH) interaction is elongated by at least 0.35Å (*endo*, pbe functional) and up to 1Å (*exo*, blyp functional). Across the Fe-(μ-SH)-Fe bridge the two Fe-(μ-SH) distances (to Fe^b, Fe^c) are *ca* 0.12Å longer than the parent Fe-(μ_3-S) distances (Table 1). Note that the *endo* isomer has shorter Fe^a--(SH) distances than does the *exo* isomer (2.86 vs 3.41), due to a weak interaction between the bridging H and Fe^a (Scheme 2): this is an agostic interaction that appears in these calculations that do not include solvation. The H--Fe^a distance is calculated as 2.39 [2.25 pbe] Å. This interaction causes Fe^a to be displaced from the plane of its three ligands (S_2Cl) by *ca* 0.4Å. The impossibility of agosticism in the *exo* isomer allows Fe^a to lie in or very close to its coordination plane.
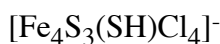

agostic *endo*   Fe-planar *endo*

Scheme 2.

In the excited states the geometrical patterns are similar, except for the *endo* isomers where the Fe spins across the SH bridge have the same parity. In these cases the Fe^a--(SH) extension is small, *ca* 0.1Å. The reason for this could be a subtle stereochemical effect controlled at S, because the Fe atoms bearing the bridge (Fe^b, Fe^c), having the same spin, are separated more than Fe^b--Fe^c with opposite spin. A general property of the stereochemistry at S is that an opening of the Fe^b-S(H)-Fe^c angle would be associated with contraction of the two Fe-S-H angles.

Table 2. Relative energies (kcal mol^{-1}) and interatomic distances (Å) for the geometrical isomers and electronic states of $[Fe_4S_3(SH)X_4]^-$. Electronic states are described in terms of the parity (opposite or same) of Fe spins supporting the μ-SH bridge, and the net spin S, using the notation {parity / S}. Entries are for functional blyp [pbe]. Fe labels follow Scheme 1.

endo/exo	electronic state	relative energy kcal mol^{-1}	Fe^a--(SH) Å	Fe^b-(SH) Fe^c-(SH) Å	Fe^b--Fe^c Å
			$[Fe_4S_3(SH)Cl_4]^-$		

endo	{opp / S=0}	0 [0]	2.86 [2.70]	2.41 [2.36] 2.48 [2.42]	2.91 [2.80]
exo	{opp / S=0}	+0.0 [+2.8]	3.41 [3.11]	2.41 [2.36] 2.44 [2.39]	2.84 [2.71]
endo	{same / S=0}	+2.2 [+2.4]	2.51 [2.46]	2.45 [2.39] 2.45 [2.39]	3.13 [2.95]
exo	{same / S=0}	+5.8 [+12.2]	3.86 [3.51]	2.45 [2.41] 2.45 [2.41]	2.88 [2.76]
endo	{opp / S=1}	+3.4 [+3.5]	2.90 [2.69]	2.30 [2.26] 2.47 [2.41]	2.94 [2.82]
exo	{opp / S=1}	+5.1 [+7.3]	3.29 [2.96]	2.29 [2.25] 2.44 [2.39]	2.84 [2.71]
endo	{same / S=1}	+8.2 [+9.5]	2.62 [2.48]	2.51 [2.46] 2.49 [2.41]	3.23 [3.08]
exo	{same / S=1}	+7.0 [+13.4]	3.80 [3.03]	2.49 [2.45] 2.49 [2.45]	3.15 [3.02]

$[Fe_4S_3(SH)(SEt)_4]^-$

endo	{opp / S=0}	0 [0]	2.87 [2.69]	2.42 [2.38] 2.49 [2.42]	2.85 [2.73]
exo	{opp / S=0}	+0.6 [+3.0]	3.48 [2.94]	2.41 [2.36] 2.44 [2.41]	2.82 [2.66]
endo	{same / S=0}	+3.5 [+4.1]	2.59 [2.49]	2.46 [2.40] 2.48 [2.42]	2.90 [2.75]
exo	{same / S=0}	+8.0 [+9.8]	3.44 [3.04]	2.33 [2.28] 2.46 [2.37]	2.79 [2.53]

$[Fe_4S_3(SH)(SMe)_4]^-$

endo	{opp / S=0}	+0.4	2.99	2.40 2.48	2.81
exo	{opp / S=0}	0	3.37	2.40 2.44	2.77

$[Fe_4S_3(SH)(SPh)_4]^-$

endo	{opp / S=0}	+0.4 [0]	2.86 [2.71]	2.39 [2.34] 2.48 [2.42]	2.84 [2.74]
exo	{opp / S=0}	0 [+1.5]	3.38 [3.02]	2.39 [2.34] 2/44 [2.38]	2.80 [2.66]
endo	{same / S=0}	+3.5 [+2.7]	2.50 [2.45]	2.45 [2.38] 2.46 [2.39]	3.08 [2.85]

		$[Fe_4S_3(SH)(OMe)_4]^-$			
endo	{opp / S=0}	+0.8* [0]	3.39* [2.81]	2.45 [2.40] 2.47 [2.44]	2.85 [2.78]
exo	{opp / S=0}	0 [+0.3]	3.42 [3.11]	2.44 [2.38] 2.45 [2.41]	2.85 [2.72]

		$[Fe_4S_3(SH)(OPh)_4]^-$			
endo	{opp / S=0}	+0.8*	3.62	2.43 2.47	2.87
exo	{opp / S=0}	0	3.42	2.42 2.45	2.84

* Planar form of *endo* isomer: the agostic *endo* form transforms without barrier to the planar form.

Considering the results for the other X (SEt, SMe, SPh, OMe, OPh) (Table 2), the patterns of relative stability and geometry are as already described, but some additional properties are evident. There are now X ligand substituents that can have various conformations, and in the case of X=SEt these can result in energy variations of up to 1.2 kcal mol^{-1}. The *endo* {opp / S=0} structures are generally agostic (Scheme 2), but in the case of *endo* $[Fe_4S_3(SH)(SEt)_4]^-$ {opp / S=0}, there is in addition to the agostic ground state a shallow minimum at relative energy +0.4 kcal mol^{-1} where the unique Fe^a atom has planar stereochemistry and S--Fe^a is extended to 3.6Å (from 2.87Å in the agostic form). The weakly stabilising interactions between the H of *endo* μ-SH and Fe^a (and its X ligand) in agostic *endo* $[Fe_4S_3(SH)(SEt)_4]^-$ {opp / S=0} are evident in the H--Fe^a and H--S(Et) distances of 2.37 [pbe 2.17] and 2.85 [pbe 2.58]Å, and the location of Fe^a 0.48 [pbe 0.51]Å inside its S_3 coordination plane. For *endo* $[Fe_4S_3(SH)(OMe)_4]^-$ and $[Fe_4S_3(SH)(OPh)_4]^-$ in the ground {opp / S=0} electronic state the stable configuration is planar, with the H--Fe^a distances extended to 2.76 and 2.86Å respectively, while the H--O(R) distances are 2.60 (R=Me) and 3.00 (R=Ph)Å. Graphics and coordinates for the {opp / S=0} complexes in Table 2 are recorded in Supplementary Table S2.

Interconversion of *endo* and *exo* μ-SH isomers

Some structural possibilities are absent from Table 2, and this is because they undergo barrierless transformation to alternative isomers. This introduces the question of interconversion of the *endo* and *exo* isomers of $[Fe_4S_3(SH)X_4]^-$. It might appear that *endo* $\leftrightarrow$ *exo* interconversion would occur through a planar $(\mu\text{-SH})Fe_2$ transition state, but there is an alternative path with a lower barrier. The isomer interconversions occur through interchange of normal and elongated Fe-S bonds, with only slight angular movement of H. This is illustrated in Fig 2, which shows all isomers of $[Fe_4S_3(SH)(SEt)_4]^-$ (S=0) and the interconnecting transition states. The most stable *endo* opp structure is shown in the centre, while around it are the energy mininima and transition states that occur as the H-S bond is rotated around the clock face of three Fe atoms, two of which must have the same spin. The Fe-S bonds break and reform as marked. This cycle generates all isomers. The main result is that interconversions of the more stable *endo* and *exo* isomers across opposite spins have barriers of 3 - 4 kcal mol^{-1}. The excited *endo* isomer across same-signed spins has a low barrier (<1 kcal mol^{-1}) to form a more stable *exo* isomer across opposite spins. This mechanism for isomer interconversion through the breaking and making of Fe-S bonds is the same as that developed for interconversion of the configurations of μ-SH at S3B of FeMo-co (Fig 1(b)).[17]
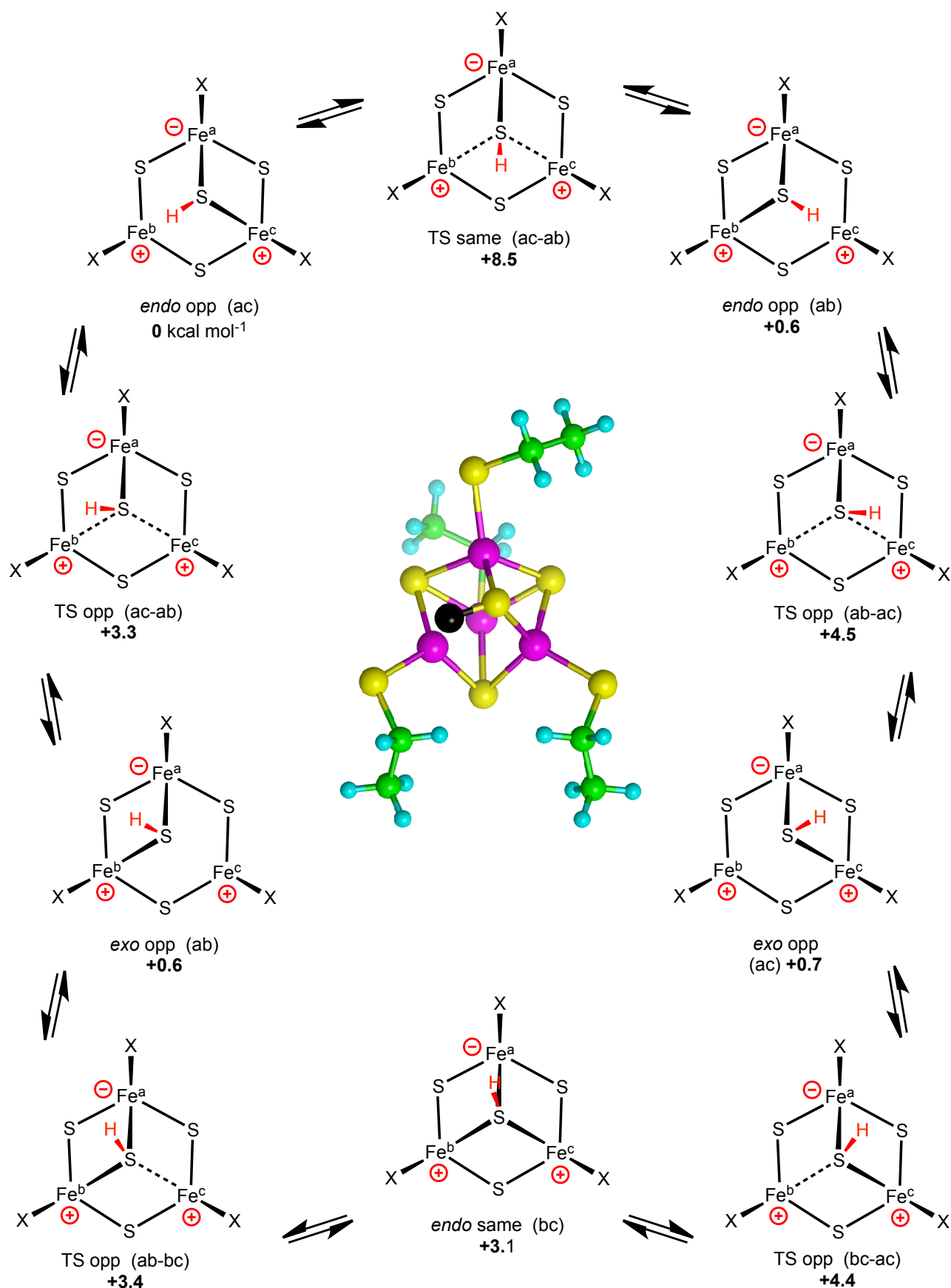
Fig. 2. The interconversions of *endo* and *exo* isomers of $[Fe_4S_3(SH)(SEt)_4]^-$. All possible isomers symbolised around the periphery are created by rotation of the H-S bond around the clock face of Fe^a, Fe^b, Fe^c: all structures have the same SEt ligand structure as the lowest energy *endo* isomer pictured in the centre (H on S is black). The signs of the spins on Fe^a, Fe^b, Fe^c are marked: TS = transition state; relative energies

are in kcal mol^{-1}. Note that the pathways involve extensions then reformations of S-Fe bonds. The excited *endo* isomer across same signed spins (bc, lower centre) has a low barrier (<1 kcal mol^{-1}) to form the more stable *exo* isomer across opposite spins (*exo opp ab*).

For $[Fe_4S_3(SH)(OMe)_4]^-$ some possible isomers are not retained by interconversion barriers, and are therefore absent from Table 2. Specifically, the *endo* {same / S=0} isomer converts without barrier to *exo* {opp / S=0}, and *exo* {same / S=0} converts without barrier to *endo* {opp / S=0}, thereby avoiding μ-SH bridges across same-signed Fe spins.

The stereochemical course of protonation of $[Fe_4S_4X_4]^{2-}$

The energy landscape for the isomers of $[Fe_4S_3(SH)X_4]^-$ probably influences the course of the protonation reaction. With recognition that actual reactions depend on the geometry of the protonating agent, and solvation, some simplified calculations have been made on the trajectories of proton addition. There are five possible approaches for a proton (Scheme 3), namely directly towards S (three equal H-S-Fe angles), or off-axis as marked for H^a (*endo* to the unique Fe), H^b (*exo* to a non-unique Fe), H^c (*endo* to a non-unique Fe), or H^d (*exo* to the unique Fe). These pathways and their products have been investigated by calculating trajectories using small-step energy minimisations (for X = Cl, OMe, SEt). The largest energy gradient is for H to bend away from the pseudo-threefold axis, towards one of the stable isomers. Approach H^b leads to *exo*-μ-SH {opp}, as expected, and similarly approach H^c proceeds to *endo*-μ-SH {opp}. Approach H^a usually leads to *endo* μ-SH {same}, while approach H^d follows various pathways, depending on the details of the H position.
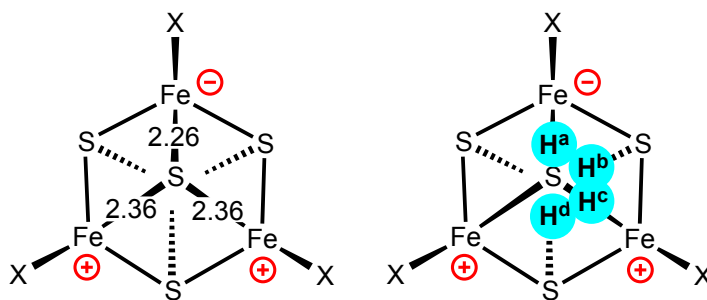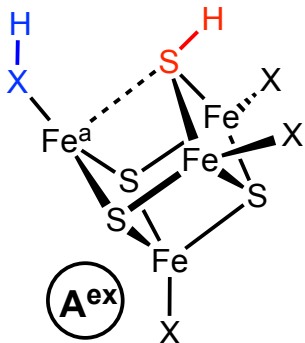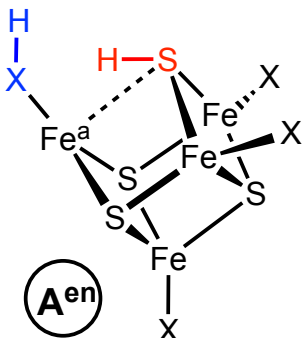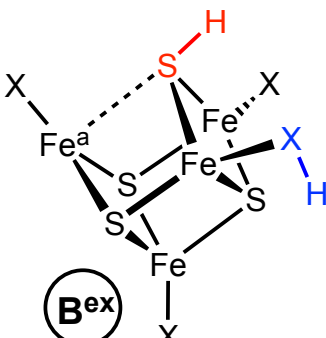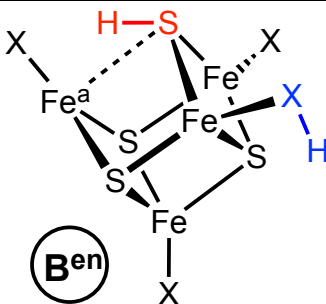

Scheme 3.

Protonation of S and X = SEt or OPh

In $[Fe_4S_4X_4]^{2-}$ clusters where X = SR or OR the most basic site is probably the ligand S or O donor atom, and therefore the consequences of prior protonation of these ligands on the subsequent protonation of μ_3-S have been investigated. There are three isomeric possibilities for the relative locations of SH and the protonated ligand, depicted in Table 3: isomer A has the protonated ligand on the unique Fe; isomer B has the protonated ligand on one of the Fe atoms supporting the μ-SH bridge; isomer C has the protonated ligand most distant, on the Fe atom opposite to SH. The main results are: (1) the ground electronic state is {opp / S=0} as usual; (2) isomer B is most stable, isomer C is ca 1 kcal mol^{-1} less stable, and isomer A is ca 6 kcal mol^{-1} less stable than B; (3) *endo* and *exo* isomers occur as usual, with longer Fe^a--S(H) in the *exo* geometry; (4) isomer rearrangements can occur, through Fe-S distance interchanges; (5) the bond to the protonated ligand, Fe-S(H)Et is lengthened by ca 0.2Å relative to Fe-SEt, and the Fe-O(H)Ph bond is lengthened by ca 0.15Å. Graphics and coordinates for the complexes in Table 3 are available in Supplementary Table S3. Some of these results (blyp) were published previously.[22]

Table 3. Isomers, relative energies (kcal mol^{-1}), and unique distances Fe^a--S(H), Fe-X(H) (Å) in doubly-protonated [Fe$_4$S$_3$(SH)(SEt)$_3$(HSEt)]^0 and [Fe$_4$S$_3$(SH)(OPh)$_3$(HOPh)]^0. Entries are for functional blyp [pbe].

| isomer	[Fe$_4$S$_3$(SH)(SEt)$_3$(HSEt)]^0 X = SEt	[Fe$_4$S$_3$(SH)(OPh)$_3$(HOPh)]^0 X = OPh
A^{ex}	+6.0 {opp / S=0} Fe--S(H) = 3.20 Fe-X(H) = 2.38 * pbe changed to **B^{ex}** {opp / S=0}	+5.8 {opp / S=0} Fe--S(H) = 3.42 Fe-X(H) = 2.12
A^{en}	+ 6.9 [+6.5] {opp / S=0} Fe--S(H) = 2.86 [2.70] Fe-X(H) = 2.42 [2.35]	** changed to **B^{ex}** {opp / S=0}
B^{ex}	0 [+1.2] {opp / S=0} Fe--S(H) = 3.29 [3.03] Fe-X(H) = 2.22 [2.19]	+1.0 [0] {opp / S=0} Fe--S(H) = 3.26 [3.06] Fe-X(H) = 2.19 [2.15]
B^{en}	+ 0.4 [0] {opp / S=0} Fe--S(H) = 3.00 [2.71] Fe-X(H) = 2.46 [2.38]	0 [+0.3] {opp / S=0} Fe--S(H) = 3.23 [3.09] Fe-X(H) = 2.20 [2.15]

(C^{ex}) structure	$+$ 1.5 [+2.7] {opp / S=0} Fe--S(H) = 3.41 [3.05] Fe-X(H) = 2.47 [2.39]	+1.0 [+2.9] {opp / S=0} Fe--S(H) = 3.50 [3.14] Fe-X(H) = 2.21 [2.16]
(C^{en}) structure	+1.3 [+0.9] {opp / S=0} Fe--S(H) = 2.98 [2.73] Fe-X(H) = 2.46 [2.38]	+2.2 [+3.4] {opp / S=0} Fe--S(H) = 3.59 [3.31] Fe-X(H) = 2.21 [2.15]

Deprotonation of [Fe$_4$S$_3$(SH)X$_4$]$^-$

All forms of [Fe$_4$S$_3$(SH)X$_4$]$^-$ revert without energy barrier to [Fe$_4$S$_4$X$_4$]$^{2-}$ when the proton is removed. This can involve substantial geometrical change: in the case of *endo* [Fe$_4$S$_3$(SH)(OPh)$_4$]$^-$ {opp / S=0} the Fe^a--S distance changes from 3.62 back to 2.37Å. The energy change during this reversion provides a measure of the energy involved in distorting the cluster and extending the Fe^a-S bond upon protonation. For example, the distance-energy potential for Fe-S bond extension in *exo* [Fe$_4$S$_3$(SH)(SEt)$_4$]$^-$ {opp / S=0} has the following values: +0.066Å, + 6 kcal mol^{-1}; + 0.29 Å, +11 kcal mol^{-1}; + 0.53Å, + 16 kcal mol^{-1}; + 1.1Å, +24 kcal mol^{-1}.

Protonation of two µ$_3$-S: [Fe$_4$S$_2$(SH)$_2$X$_4$]^0

The structural consequences of protonating two µ$_3$-S atoms of the cubanoid clusters has been calculated, for the isomers shown in Scheme 4. These structures, which have two severed Fe-S bonds and two three-coordinate Fe atoms, are calculated to be stable. Additional isomers are possible (see Supplementary Table S4 for further information). It is recognised that the basicities of the remaining µ$_3$-S atoms will be substantially diminished after protonation of the first, and also that the [Fe$_4$S$_2$(SH)$_2$X$_4$]^0 structures are likely to have enhanced reactivity and to react further in solution, but the calculations show that they can reside in local energy minima.

exo, exo   *endo, exo*

endo, endo   *endo, exo*
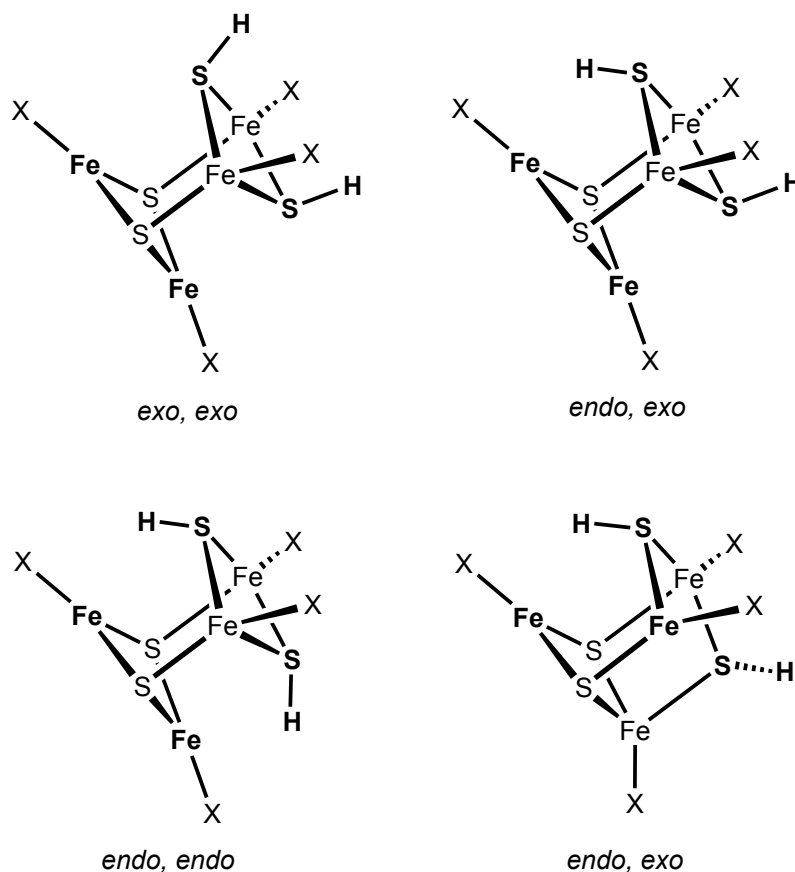
Scheme 4. Four of the possible isomers for doubly-protonated $[Fe_4S_2(SH)_2X_4]^0$

Protonation of $[Fe_4Q_4X_4]^{2-}$, Q = O, Se, Te

Another question: does the propensity of μ_3-S to convert to μ-SH upon protonation extend to other μ_3-Q in the homologous cubanoid chalcogenide clusters $[Fe_4Q_4X_4]^{2-}$? This has been investigated by optimising $[Fe_4Q_3(QH)(SEt)_4]^-$ structures (S=0) with a proton in the symmetrical μ_3-QH position of optimised $[Fe_4Q_4(SEt)_4]^{2-}$. In the case of Q = O only one energy minimum has been located for $[Fe_4O_3(OH)(SEt)_4]^-$, and it retains a symmetrical μ_3-OH bridge. *Endo* or *exo* structures with a μ-OH bridge, analogous to the μ-SH bridging forms of $[Fe_4S_3(\mu$-SH$)(SEt)_4]^-$, are unstable relative to that with symmetrical μ_3-OH. In the case of Q = Se, the symmetrical μ_3-SeH bridge is unstable relative to the *endo* and *exo* isomers, and the geometrical and electronic states of $[Fe_4Se_3(\mu$-SeH$)(SEt)_4]^-$ are homologous to those of $[Fe_4S_3(\mu$-SH$)(SEt)_4]^-$. With Q = Te, *exo* $[Fe_4Te_3(\mu$-TeH$)(SEt)_4]^-$ is similar to its homologues, but in *endo* $[Fe_4Te_3(\mu$-TeH$)(SEt)_4]^-$ the agostic Te-H-Fe interaction reaches its limit as Te-H-Fe bridge bonding (Scheme 5, and Supplementary Table S5). In the series of agostic *endo* $[Fe_4Q_3(QH)(SEt)_4]^-$ isomers with Q = S, Se, Te, the H--Fe[a] interaction decreases in length as 2.38 [pbe 2.16], 2.23 [pbe 2.13], 1.90 [pbe 1.84] respectively.

Scheme 5. *Exo* and *endo* $[Fe_4Te_3(\mu\text{-}TeH)(SEt)_4]^-$.

Discussion

The principal results are summarised as:

(1) protonation of a μ_3-S atom in cubanoid clusters $[Fe_4S_4X_4]^{2-}$ does not lead to triply-bridging SH, but instead forms a μ-SH bridge as a consequence of severe weakening of one S-Fe bond;

(2) the structural rearrangement associated with protonation is reversible;

(3) the unique Fe atom in $[Fe_4S_3(SH)X_4]^-$ is three-coordinate, with planar or approximately planar stereochemistry;

(4) there are two geometrical isomers of $[Fe_4S_3(SH)X_4]^-$, *endo* and *exo*, in which the pyramidal μ-S-H is directed towards or away from the unique Fe atom;

(5) there is negligible energy difference between the *endo* and *exo* isomers;

(6) the most stable electronic state of $[Fe_4S_3(SH)X_4]^-$ has S=0 and oppositely-signed spin densities (ca 3e) on the two Fe atoms bearing the μ-SH bridge;

(7) excited states with same-signed spin densities across the bridge occur at energies of 2 - 8 kcal mol^{-1};

(8) interconversions between *endo* and *exo* isomers, and ground and excited states, occur through concerted lengthenings and shortenings of Fe-S(H) interactions, not through inversion of μ-SH;

(9) the energy surfaces for isomer interconversions are relatively flat;

(10) protonation of an X ligand does not change the characteristics of protonation of μ_3-S.

It needs to be remembered that these calculations describe rarefied behaviour in the gas phase, for mainly anionic clusters.   In real solutions the effects of solvation, of associated counter ions, and of the conjugate bases of the protonating agents, are expected to be of similar or larger energies: these variables could determine the actual species that exist in solution and are isolable.

Testing the theory

This theoretical description provides a new dimension to the chemistry of long-known $[Fe_4S_4X_4]^{2-}$ clusters, and this theory demands experimental testing, verification, and elaboration.   So far the main experimental verification derives from the kinetic measurements of the proton catalysed substitution reactions of $[Fe_4S_4X_4]^{2-}$ made by Henderson and colleagues.[19,20]   Recognition that protonation opens up the cluster and creates an under-coordinated Fe site was the clue to the development of a general mechanism of catalysis that accounts for all of the kinetic data.[21]   The essence of the mechanism for the substitution of $[Fe_4S_4X_4]^{2-}$ by PhSH, as catalysed by the acid Et_3NH^+ in acetonitrile, is shown in Fig 3: this mechanistic insight allows satisfactory explanation of previously enigmatic results.[22]   In this context it is noted that the opening of the cluster on protonation, and generation of an under-coordinated Fe atom, has implications for other aspects of the reactivity of these clusters, such as cluster condensation reactvity:[42] there is also some similarity with the open and closed forms of the P-cluster of nitrogenase.[43]
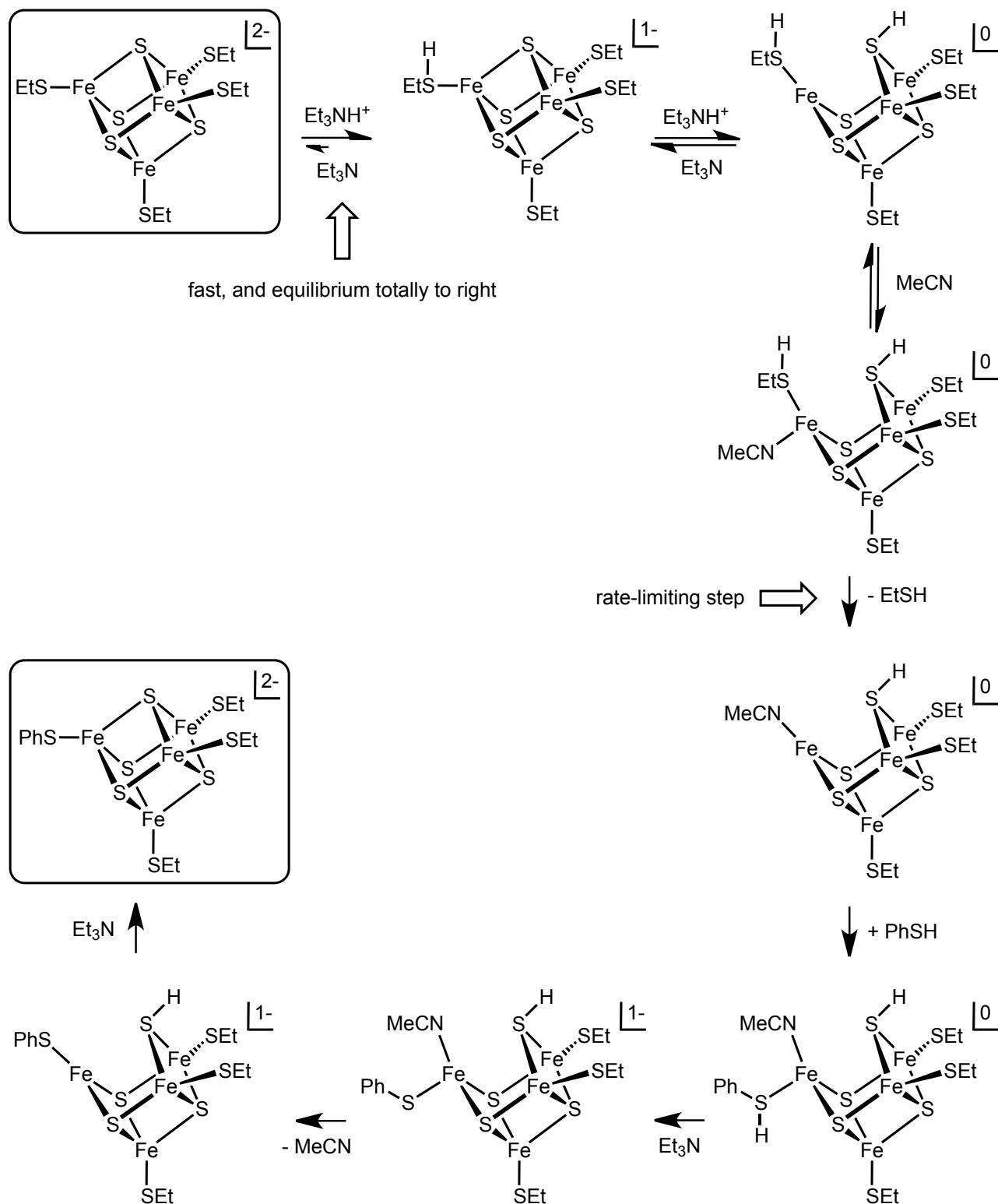
Fig. 3. The essence of the mechanism proposed for the substitution of $[Fe_4S_4(SEt)_4]^{2-}$ by PhSH, as catalysed by the acid Et_3NH^+ (adapted from ref [22] which includes full experimental details).

Definitive verification of the theory would be afforded by preparation and crystallisation of a complex of type $[Fe_4S_3(SH)X_4]^-$, or of type $[Fe_4S_3(SH)(SR)_3(HSR)]^0$, followed by diffraction analysis. To my knowledge no such relevant complex has been isolated or crystallised, and the Cambridge Structural Database is devoid even of related species: the closest structural analog is $[(Cp^*Ir)_3(\mu_3\text{-S})_3(\mu\text{-SH})PdCl(PPh_3)]$, which is chemically very different, and which was not generated by protonation of μ_3-S.[44]

$$[(Cp^*Ir)_3(\mu_3\text{-}S)_3(\mu\text{-}SH)PdCl(PPh_3)]$$
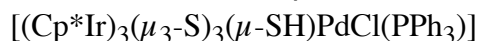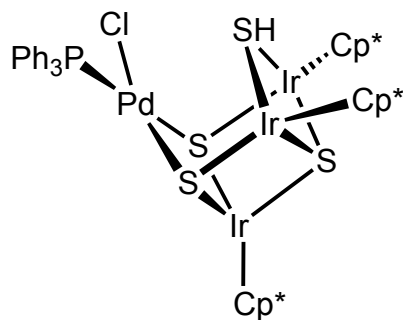
How could $[Fe_4S_3(SH)(SR)_4]^-$ or $[Fe_4S_3(SH)(SR)_3(HSR)]^0$ be synthesised and crystallised? To aid crystallisation it is advisable to use phenyl or aryl substituents. The reason for this derives from the disproportionately large number of such phenylated compounds in the Cambridge Structural Database, particularly monoanions crystallised with Ph_4P^+ or Ph_4As^+, a phenomenon that can be traced to the occurrence of intermolecular phenyl (and aryl) embraces that control the crystal packing.[45-49] Therefore designed target compounds would be such as $Ph_4P^+[Fe_4S_3(SH)(SPh)_4]^-$ or $[Fe_4S_3(SH)(SPh)_3(PhSH)]$, generated in aprotic solvent systems such as acetonitrile. The protonating agent needs to be sufficiently acidic, and to have a non-coordinating conjugate base: it is suggested that tertiary ammonium salts $R^1R^2R^3NH^+BF_4^-$ would be suitable, where one or two of the substituents are aryl (to confer appropriate acidity), and that the volume of the three substituents be sufficient to ensure that $R^1R^2R^3N$ is unable to coordinate the unique Fe atom. It is possible that resulting crystals would retain $R^1R^2R^3N$, hydrogen bonded to the μ-SH group of the target compound.

What acidity is required at the protonating agent? The electrochemical data of Nakamoto *et al* for $[Fe_4X_4(YAr)_4]^{2-}$ (X, Y = S, Se) in aqueous solution indicate that the pK_a values of X and Y are in the range 5.8 - 8.8.[50] Control of the stoichiometry of protonation is needed, to avoid the decomposition (to H_2S) long-known as the 'acid-lability' of FeS proteins.[1]

Another synthetic target type could be **1**, in which an added ligand Z completes four-coordination of the unique Fe atom. Ligand Z should be non-basic, and not phosphine (with desulfurisation properties): halide or pseudo-halide ions could be suitable as Z. Protonation of X in **1** is possible. To be more specific, PhS is recommended for X, and so suggested compounds to target are $(Ph_4P^+)_2[ClFe_4S_3(SH)(SPh)_4]^{2-}$, $Ph_4P^+[ClFe_4S_3(SH)(SPh)_3(PhSH)]^-$.

1
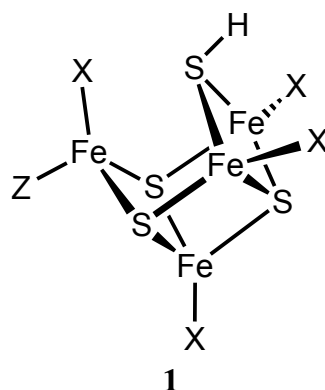
Another approach to experimental verification deploys voltammetry, because two chemical (C) steps – protonation of μ_3-S and separation of the unique three-coordinate Fe atom from μ-SH – are coupled to electron transfer (E). Electron-transfer potentials for the protonated cluster are expected to shift appreciably relative to the unprotonated form. Therefore, variable scan rate cyclic voltammetry on mixtures of $[Fe_4S_4X_4]^{2-}$ and stoichiometric proportions of $R^1R^2R^3NH^+BF_4^-$ (with supporting electrolyte unreactive in this context) should be informative about the thermodynamics and kinetics of the coupled E/C steps. Related experiments have been reported by Nakamoto[51,50,52]

on [Fe$_4$S$_4$X$_4$] complexes, and reports of the proton-gated voltammetry of [Fe$_3$S$_4$] proteins are also relevant, albeit with a different cluster core.[53-57]

Finally, I have proposed that the mechanism by which the oxygen-tolerant [NiFe] hydrogenase enzymes reverse the direction of electron flow, changing from one-electron oxidation of H$_2$ to two-electron (and more) reduction of O$_2$,[58,59] is triggered by protonation of the proximal cluster [Fe$_4$S$_3$(S-cys)$_6$] such that its electron-transfer potentials are altered.[60] While this is a different cluster system, the chemical principles are based on the theory presented here, and specifically protonation of a μ_3-S atom with concomitant severance of an S-Fe upon formation of μ-SH. I have suggested testing experiments for the oxygen-tolerant [NiFe] hydrogenase mechanism, which, if successful, will contribute to validation of the theory presented in this paper.

Acknowledgements

TOC graphic
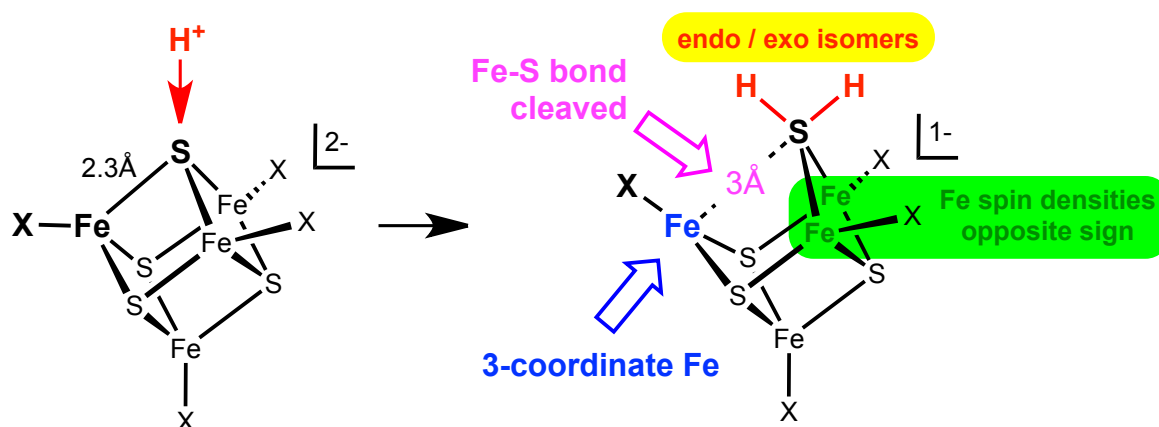
References

1   W. H. Orme-Johnson, Annual Review of Biochemistry, 1973, 42, 159-204.

2   R. H. Holm, Chem. Soc. Rev., 1981, 10, 455-490.

3   R. H. Holm, P. Kennepohl and E. I. Solomon, Chem. Rev., 1996, 96, 2239-2314.

4   H. Beinert, R. H. Holm and E. Munck, Science, 1997, 277, 653-659.

5   P. Venkateswara Rao and R. H. Holm, Chemical Reviews, 2004, 104, 527-560.

6   S. C. Lee, W. Lo and R. H. Holm, Chemical Reviews, 2014, 114, 3579-3600.

7   B. K. Burgess and D. J. Lowe, Chem. Rev., 1996, 96, 2983-3011.

8   B. E. Smith, Adv. Inorg. Chem., 1999, 47, 159-218.

9   R. Y. Igarashi and L. C. Seefeldt, Crit. Rev. Biochem. Mol. Biol., 2003, 38, 351-384.

10   D. C. Rees, F. A. Tezcan, C. A. Haynes, M. Y. Walton, S. Andrade, O. Einsle and J. A. Howard, Phil. Trans. Roy. Soc. A, 2005, 363, 971-984.

11   J. B. Howard and D. C. Rees, Proc. Nat. Acad. Sci. USA, 2006, 103, 17119-17124.

12   L. C. Seefeldt, B. M. Hoffman and D. R. Dean, Annu. Rev. Biochem., 2009, 78, 701-722.

13   Z.-Y. Yang, K. Danyal and L. C. Seefeldt, Methods Mol. Biol., 2011, 766, 9-29.

14   Y. Hu and M. Ribbe, JBIC Journal of Biological Inorganic Chemistry, 2014, 19, 731-736.

15   O. Einsle, JBIC Journal of Biological Inorganic Chemistry, 2014, 19, 737-745.

16   I. Dance, Dalton Trans., 2012, 41, 7647-7659.

17   I. Dance, Inorg Chem, 2013, 52, 13068-13077.

18   I. Dance, Chem Commun (Camb), 2013, 49, 10893-10907.

19   R. A. Henderson, Coord. Chem. Rev., 2005, 249, 1841-1856.

20   R. A. Henderson, Chem. Rev., 2005, 105, 2365-2437.

21   A. Alwaaly, I. Dance and R. A. Henderson, Chemical Communications, 2014, 50, 4799-4802.

22   I. Dance and R. A. Henderson, Dalton Transactions, 2014, 43, 16213-16226.

23   C. C. D. Centre, http://www.ccdc.cam.ac.uk, 2014.

24   J. R. Long, L. S. McCarty and R. H. Holm, J. Am. Chem. Soc., 1996, 118, 4603-4616.

25   Y.-H. Qin, M.-M. Wu and Z.-N. Chen, Acta Crystallographica Section E, 2003, 59, m317-m318.

26   L. Han, L.-X. Shi, L.-Y. Zhang, Z.-N. Chen and M.-C. Hong, Inorganic Chemistry Communications, 2003, 6, 281-283.

27   S. Kuwata and M. Hidai, Coord. Chem. Rev., 2001, 213, 211-305.

28   B. Delley, J. Chem. Phys., 1990, 92, 508-517.

29   B. Delley, in Modern density functional theory: a tool for chemistry, eds. J. M. Seminario and P. Politzer, Elsevier, Amsterdam, 1995, p. 221-254

30   B. Delley, J. Chem. Phys., 2000, 113, 7756-7764.

31   G. C. Papaefthymiou, E. J. Laskowski, S. Frota-Pessoa, R. B. Frankel and R. H. Holm, Inorg. Chem., 1982, 21, 1723-1728.

32   R. A. Torres, T. Lovell, L. Noodleman and D. A. Case, Journal of the American Chemical Society, 2003, 125, 1923-1936.

33   L. Noodleman, C. Y. Peng, D. A. Case and J. M. Mouesca, Coord. Chem. Rev., 1995, 144, 199-244.

34   I. Dance, Molecular Simulation, 2008, 34, 923-929.

35   I. Dance, Molecular Simulation, 2011, 37, 257.

36   B. A. Averill, T. Herskovitz, R. H. Holm and J. A. Ibers, J.Am.Chem, 1973, 95, 3523-3534.

37   L. Que, M. A. Bobrik, J. A. Ibers and R. H. Holm, J. Am. Chem. Soc., 1974, 96, 4168-4178.

38   M. A. Bobrik, K. O. Hodgson and R. H. Holm, Inorganic Chemistry, 1977, 16, 1851-1858.

39   E. J. Laskowski, J. G. Reynolds, R. B. Frankel, S. Foner, G. C. Papaefthymiou and R. H. Holm, J.Am.Chem.Soc., 1979, 101, 6562-6570.

40   H. Wong, M. A. Bobrik and R. H. Holm, Inorg.Chem., 1978, 17, 578-574.

41   E. J. Laskowski, R. B. Frankel, W. O. Gillum, G. C. Papaefthymiou, J. Renaud, J. A. Ibers and R. H. Holm, J.Am.Chem.Soc., 1978, 100, 5322-5337.

42   Y. Ohki and K. Tatsumi, Zeitschrift Fur Anorganische Und Allgemeine Chemie, 2013, 639, 1340-1349.

43   J. W. Peters, M. H. B. Stowell, S. M. Soltis, M. G. Finnegan, M. K. Johnson and D. C. Rees, Biochemistry, 1997, 36, 1181-1187.

44   A. Shinozaki, H. Seino, M. Hidai and Y. Mizobe, Organomet., 2003, 22, 4636-4638.

45   I. Dance and M. Scudder, Chem. Eur. J., 1996, 2, 481-486.

46   M. Scudder and I. Dance, J. Chem. Soc., Dalton Trans., 1998, 3167-3176.

47   M. Scudder and I. Dance, J. Chem. Soc., Dalton Trans., 1998, 3155-3166.

48   M. Scudder and I. Dance, J. Chem. Soc., Dalton Trans., 1998, 329-344.

49   I. Dance and M. Scudder, CrystEngComm, 2009, 11, 2233-2247.

50   M. Nakamoto, K. Tanaka and T. Tanaka, Bulletin of the Chemical Society of Japan, 1988, 61, 4099-4105.

51   M. Nakamoto, K. Tanaka and T. Tanaka, J. Chem. Soc., Chem. Comm., 1986, 1669-1670.

52   M. Nakamoto, K. Fukaishi, T. Tagata, H. Kambayashi and K. Tanaka, Bulletin of the Chemical Society of Japan, 1999, 72, 407-414.

53   B. Shen, L. L. Martin, J. N. Butt, F. A. Armstrong, C. D. Stout, G. M. Jensen, P. J. Stephens, G. N. La Mar, C. M. Gorst and B. K. Burgess, Journal of Biological Chemistry, 1993, 268, 25928-25939.

54   J. N. Butt, A. Sucheta, L. L. Martin, B. Shen, B. K. Burgess and F. A. Armstrong, Journal of the American Chemical Society, 1993, 115, 12587-12588.

55   J. L. C. Duff, J. L. J. Breton, J. N. Butt, F. A. Armstrong and A. J. Thomson, Journal of the American Chemical Society, 1996, 118, 8593-8603.

56   J. N. Butt, S. E. J. Fawcett, J. Breton, A. J. Thomson and F. A. Armstrong, Journal of the American Chemical Society, 1997, 119, 9729-9737.

57   J. Hirst, G. N. L. Jameson, J. W. A. Allen and F. A. Armstrong, Journal of the American Chemical Society, 1998, 120, 11994-11999.

58   J. Fritsch, O. Lenz and B. Friedrich, Nat Rev Micro, 2013, 11, 106-114.

59   W. Lubitz, H. Ogata, O. Rüdiger and E. Reijerse, Chemical Reviews, 2014, 114, 4081-4148.

60   I. Dance, Chem. Sci., 2015, 6, 1433-1443.